https://doi.org/10.5194/egusphere-2023-152
Preprint. Discussion started: 2 February 2023

High resolution CMAQ simulations of ozone exceedance events during the Lake Michigan Ozone Study

R. Bradley Pierce[1], Monica Harkey[4], Allen Lenzen[1], Lee M. Cronce[2], Jason A. Otkin[1,2], Jonathan L. Case[3], David S. Henderson[1], Zac Adelman[5], Tsengel Nergui[5], Christopher R. Hain[6]

[1]Space Science and Engineering Center, University of Wisconsin-Madison, Madison, 53706, USA
[2]Cooperative Institute for Meteorological Satellite Studies, University of Wisconsin, Madison, Madison, 53706, USA
[3]ENSCO, Inc., NASA Short-term Prediction Research and Transition Center, Huntsville, 35805, USA
[4]Center for Sustainability and the Global Environment, University of Wisconsin-Madison, Madison, 53706, USA
[5]Lake Michigan Air Directors Consortium, Hillside, 60162, USA
[6]Earth Science Office, NASA Marshall Space Flight Center, Huntsville, 35808, USA

Correspondence to: R. Bradley Pierce (rbpierce@wisc.edu)

Abstract: We evaluate two high-resolution Lake Michigan air quality simulations during the 2017 Lake Michigan Ozone Study campaign. These air quality simulations employ identical chemical configurations but use different input meteorology. The "EPA" configuration follows EPA recommended modeling practices, whereas the "YNT_SSNG" employs different parameterization schemes and satellite-based inputs of sea surface temperatures, green vegetative fraction, and soil moisture and temperature. Overall, we find similar performance in model simulations of hourly and daily 8-hour maximum (MDA8) ozone, with the EPA and YNT_SSNG simulations showing biases of -13.31 and -13.54 ppbv, respectively during periods when the observed MDA8 was greater than 70ppbv. However, for the two monitoring sites that observed high ozone events, the EPA simulation better matched observations at Sheboygan KA and the YNT_SSNG simulation better matched observations at Chiwaukee Prairie. We find differences between the two simulations are largest for column amounts of ozone precursors, particularly NO_2. Across three high ozone events, the YNT_SSNG simulation has a lower column NO_2 bias (0.17×10^{15} molecules/cm^2) compared to the EPA simulation (0.35×10^{15} molecules/cm^2). The YNT_SSNG simulation also has an advantage in better capturing the structure of the boundary layer and lake breeze during the June 2 high ozone event, although the timing of the lake breeze is about 3 hours too early. Our results are useful in informing an air quality modeling framework for the Lake Michigan area.

1. Introduction

Ground-level ozone has many well-documented effects on human health, including increased risk for respiratory and cardiovascular diseases, and even premature death (Di et al., 2017; Lelieveld et al., 2015; Manisalidis et al., 2020). Ozone also damages plant tissue, affecting crop health (e.g. Clifton et al., 2020; Shindell et al., 2012). Ground-level ozone is formed by photochemical reactions between nitrogen oxides (NOx) and volatile organic compounds (VOCs); major NOx sources include fuel combustion, biomass burning, soil microbes, and lightning, with anthropogenic sources dominant (Hall et al, 1996; Juncosa Calahorrano et al., 2021; Lamsal et al., 2010; Lawrence and Crutzen, 1999; Nault et al., 2017), major sources of VOCs include industrial processes and natural sources, such as trees (Guenther et al., 1995; He et al., 2019).

Since the first National Ambient Air Quality Standard (NAAQS) for ozone was released in 1979, most lakeshore counties in the states bordering Lake Michigan (Wisconsin, Illinois, Indiana, and Michigan) have been designated as being in nonattainment for surface ozone in one or more of the subsequent NAAQS revisions. These states are required by the Clean Air Act to develop State Implementation Plans (SIPs) to demonstrate strategies to bring affected areas into attainment and to mitigate the impacts of high ozone concentrations. Large decreases in local emissions of ozone precursors have steadily reduced one- and eight-hour maximum ozone concentrations across the region in recent decades (Adelman 2020). However, the implementation of stricter ozone NAAQS, along with increases in susceptible populations (e.g. Daggett et al., 2000), means that additional air quality modeling assessments are necessary to help states demonstrate that they can reach attainment by the required statutory deadlines.

https://doi.org/10.5194/egusphere-2023-152
Preprint. Discussion started: 2 February 2023

The areas along the Lake Michigan shoreline are susceptible to high ozone amounts because of a combination of abundant precursor emissions and transport processes, particularly the lake breeze circulation. The relationships between area emissions and meteorology as they impact air quality have been characterized in field campaigns (Sexton and Westberg, 1980; Dye et al., 1995; Foley et al., 2011; Stanier et al., 2021), and the meteorological component is the subject of Part 1 of this study (Otkin et al., 2022). Ozone concentrations along coastlines can be enhanced significantly when urban emissions react within the shallow, stable, marine boundary layer (Fast and Heilman, 2003). The lake breeze circulation is particularly important for enhanced ozone production over Lake Michigan where it contributes to roughly 80% of high ozone episodes observed in eastern Wisconsin (Lennartson and Schwartz, 2002; Cleary et al., 2021).

As highlighted by Dye et al. (1995), there has been a need for a modeling framework that represents the finer scales of emissions transport and chemistry near the Lake Michigan shoreline. Developing emission control strategies to mitigate these coastal high ozone events requires accurate prediction of the lake breeze transport processes at scales of 1-10 km. These chemical transport processes cannot be accurately resolved using the 12-km resolution meteorological and chemical simulations typically used in air quality modeling for previous SIPs.

We have developed a high-resolution, satellite-constrained meteorological modeling platform for the Midwest United States that supports the needs of the Lake Michigan Air Directors Consortium (LADCO) as they conduct detailed air quality modeling assessments for its member states. In part I of this study, Otkin et al. (2022) assessed the impact of different high-resolution surface datasets, parameterization schemes, and analysis nudging on near-surface meteorological conditions and energy fluxes relative to the model configuration and input datasets typically employed by the Environmental Protection Agency (EPA). In part II of this study, we use meteorological output obtained from two of these simulations, as input to the EPA Community Multiscale Air Quality (CMAQ) model version 5.2.1 (Byun and Schere, 2006; Nolte et al., 2015) model simulations to assess the impact of these model changes on ozone forecasts in the Lake Michigan region. The remainder of this paper is organized as follows. Section 2 contains a description of the CMAQ model configurations and observational data used for evaluation. Results are presented in Section 3, with discussion and conclusions provided in Section 4.

2. Methods

In this work, we compare two CMAQ simulations, one with EPA meteorology, and the other with meteorology from our optimized WRF configuration, as detailed in Part I (Otkin et al., 2022). Both sets of meteorological simulations employ a triple-nested domain configuration containing 12-, 4-, and 1.3-km resolution grids, respectively (Figure 1 in Otkin et al., 2022), as well as RRTMG longwave and shortwave radiation (Iacono et al. 2008; Mlawer et al. 1997) and the Kain-Fritsch cumulus scheme (Kain 2004) on the outer two domains. The EPA simulation employs the Morrison microphysics (Morrison et al. 2005), ACM2 PBL (Pleim 2007), and the Pleim-Xu LSM (Gilliam and Pleim 2010; Xiu and Pleim, 2001) parameterization schemes, with indirect soil moisture and soil temperature nudging. Our optimized meteorological modeling platform uses the YSU PBL (Hong et al. 2006), Noah LSM (Chen and Dudhia, 2001; Ek et al. 2003), and Thompson microphysics (Thompson et al. 2008, 2016) schemes, constrained by high-resolution (1km) soil moisture and temperature analyses (Case 2016; Case and Zavodsky 2018; Blankenship et al. 2018) from the Short-term Prediction Research and Transition Center (SPoRT), daily high resolution (1.3 km) Great Lakes surface temperatures (Schwab 1992) from the Great Lakes Surface Environmental Analysis (GLSEA), and high resolution (4 km) Green Vegetation Fraction (GVF) from the Visible Infrared Imaging Radiometer Suite (VIIRS; Vargas et al. 2015) in place of monthly GVF climatologies. This optimized configuration is hereafter referred to as the YNT_SSNG. Otkin et al. (2022) found that the EPA configuration generally produced more accurate meteorological analyses on the 12-km domain, but its accuracy decreased with finer model grid resolution. In contrast, the YNT_SSNG statistics showed consistent reductions in RMSE for 2-m temperature, 2-m water vapor mixing ratio, and 10-m wind speed relative to the EPA as the model resolution increased from 12 km to 1.3 km.

Each CMAQ simulation is run with the same configuration and anthropogenic emissions. Our configuration includes "AERO6" aerosol chemistry, the Carbon Bond 6 chemical mechanism (Emery et al., 2015; Luecken et al., 2019), and in-line photolysis. CMAQ was run with 39 vertical layers with a top of approximately 100 hPa, thus using all available layers from our WRF simulations. As with our WRF simulations, we ran CMAQ on three domains: one using 12 km by 12 km horizontal resolution over the continental U.S. (396 x 246 grid points), one using 4 km by 4 km horizontal

https://doi.org/10.5194/egusphere-2023-152
Preprint. Discussion started: 2 February 2023

resolution over the upper Midwest (447 x 423 grid points), and one using 1.3 km by 1.3 km horizontal resolution over Lake Michigan and nearby areas (245 x 506 grid points). The 12 km CMAQ simulations employ lateral boundary conditions from the Real-time Air Quality Modeling System (RAQMS) model (Pierce et al., 2007), which includes assimilation of ozone retrievals from the Microwave Limb Sounder (MLS) and Ozone Monitoring Instrument (OMI) on the NASA Aura satellite and assimilation of aerosol optical depth (AOD) from the Moderate Resolution Imaging Spectroradiometer (MODIS) on the NASA Terra and Aqua satellites. The 4-km and 1.3-km simulations employ lateral boundary conditions from the respective parent grid.

Anthropogenic emissions for the 12 km domain were taken from the 2016 National Emissions Inventory Collaborative (NEIC, 2019), version 1. Anthropogenic emissions for the 4 km and 1.3 km domains were taken from the 2017 National Emissions Inventory, version 1 (US EPA, 2021; Adams, 2020), where emissions on the 4 km domain were provided by the EPA (Kirk Baker, personal communication), and then interpolated and downscaled by $1/9^{th}$ for use on the 1.3 km domain. Biogenic emissions were calculated using the Biogenic Emission Inventory System (BEIS) with the Biogenic Emissions Landuse Database, version 3 (BELD3; Carlton and Baker, 2011). Meteorologically-sensitive input for in-line biogenic emissions calculations (such as frost dates) were generated separately for each set of CMAQ simulations using Sparse Matrix Operator Kernel Emissions (SMOKE) programs. As biogenic emissions are calculated in-line, they vary among our configurations with differing input GVF.

We focus on the innermost, 1.3 km domain surrounding Lake Michigan, during the 2017 Lake Michigan Ozone Study (LMOS) field campaign (Stanier et al., 2021) which occurred from 22 May –22 June 2017. Our chemical evaluation focuses on ozone and two of its precursors, nitrogen dioxide and formaldehyde, in the surface layer and in the atmospheric column. We employ ozone observations from the Air Quality System (AQS) monitoring network, using the Atmospheric Model Evaluation Tool (AMET) developed by the EPA. We also utilize nitrogen dioxide (NO_2) and formaldehyde (HCHO) in situ observations from an EPA trailer that was deployed at Sheboygan, WI, and in situ O_3 and wind observations at select monitors that were submitted to the LMOS data repository (https://asdc.larc.nasa.gov/soot/power-user/LMOS/2017). For column evaluation, we employ observations of column NO_2 and HCHO from the Geostationary Trace Gas Aerosol Sensor Optimization (GeoTASO; Leitch et al., 2014) instrument taken during LMOS (Judd et al., 2019).

3. Results

Our model comparison is organized by three time periods. We first evaluate model performance of the EPA and YNT_SSNG simulations over the entire LMOS period, based on the ozone precursors of NO_2 and HCHO, as well as daily 8-h maximum ozone. Used in the NAAQS for ozone, maximum 8-hour ozone amounts are calculated as a rolling 8-h average for each day, starting for the period of 7 am to 3 pm local standard time (LST), and ending with the period of 11 pm to 7 am LST the following day. However, 8-h maximum ozone is strongly influenced by days with low and moderate ozone concentrations. Though only 5.9% (112) of the 8-hour maximum ozone periods within the 1.3 km domain were above the NAAQS threshold for ozone (70 ppbv) during LMOS (see Fig. 1), it is these higher 8-h maximum ozone values that are most relevant to SIP modeling.

To evaluate the simulations more precisely, we then evaluate the high ozone days as identified by the two coastal AQS monitors that tend to show the highest ozone concentrations. High ozone days with extensive observations during LMOS 2017 include: 2-4 June, 9–12 June, and 14–16 June (Abdi-Oskouei et al., 2020) and are referred to as events A, B, and C, respectively. Finally, we evaluate model performance over the broader western Lake Michigan shoreline area during the only ozone exceedance event on 2 June.

3.1 Model performance over the entire LMOS period

3.1.1 8-hour maximum ozone

Figure 1 shows binned whisker plots of 8-h maximum ozone bias and RMSE at 10 ppb intervals for the 1.3km simulations for all sites within the 1.3km domain. Systematic high biases for lower ozone concentrations (< ~40 ppbv) and a low bias for higher ozone concentrations (> 50 ppbv) are evident in both simulations. However, the YNT_SSNG simulations show smaller biases and RMSE than the EPA for 8-h maximum ozone concentrations between 40-70 ppbv. Both simulations show similar biases and RMSE within the 70-80 ppbv bin and the EPA shows significantly

https://doi.org/10.5194/egusphere-2023-152
Preprint. Discussion started: 2 February 2023

lower biases and RMSE in the 80-90 ppbv bin. Figure 2 shows the geographical distribution of 8-h maximum ozone bias and RMSE for the 1.3km EPA and YNT_SSNG for all AQS sites within the 1.3km domain. Overall biases are largely negative, reflecting underestimates of 8-h maximum ozone at the AQS sites. When compared on a site-by-site basis, the biases and RMSE in 8-h maximum ozone are generally smaller by more than 2 ppbv in the YNT_SSNG simulation.

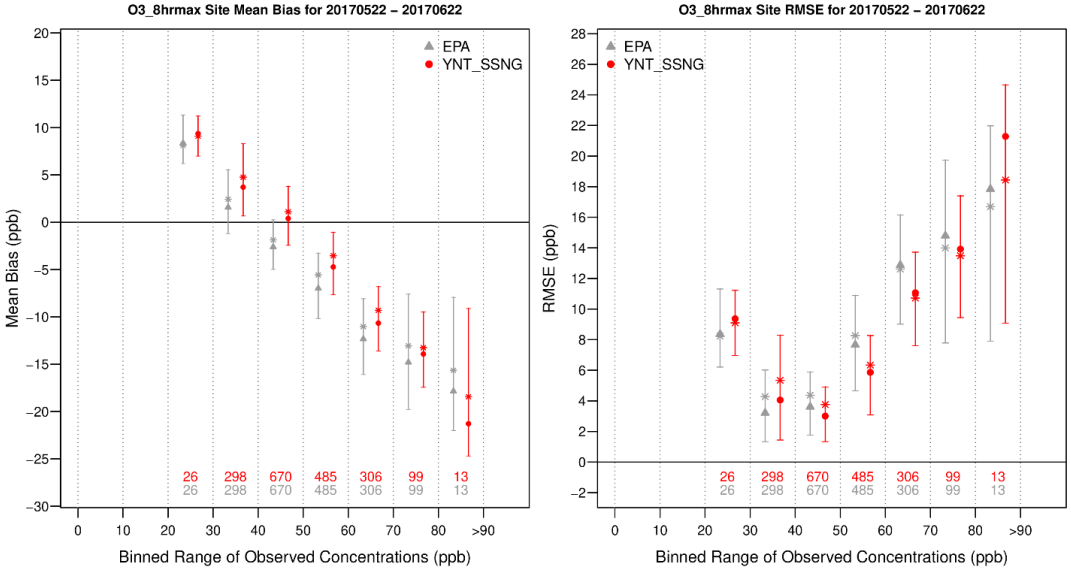

Figure 1. Whisker plots showing the bias (left) and RMSE (right) for binned 8-h maximum ozone concentrations from the EPA (gray) and YNT_SSNG (red) CMAQ simulations using hourly data within the 1.3km domain during the LMOS period of record from 22 May 2017 to 22 June 2017. Triangles and circles represent the conditional distribution medians, stars represent distribution means, and lines and whiskers represent the Q1 to Q3 ranges.

https://doi.org/10.5194/egusphere-2023-152
Preprint. Discussion started: 2 February 2023

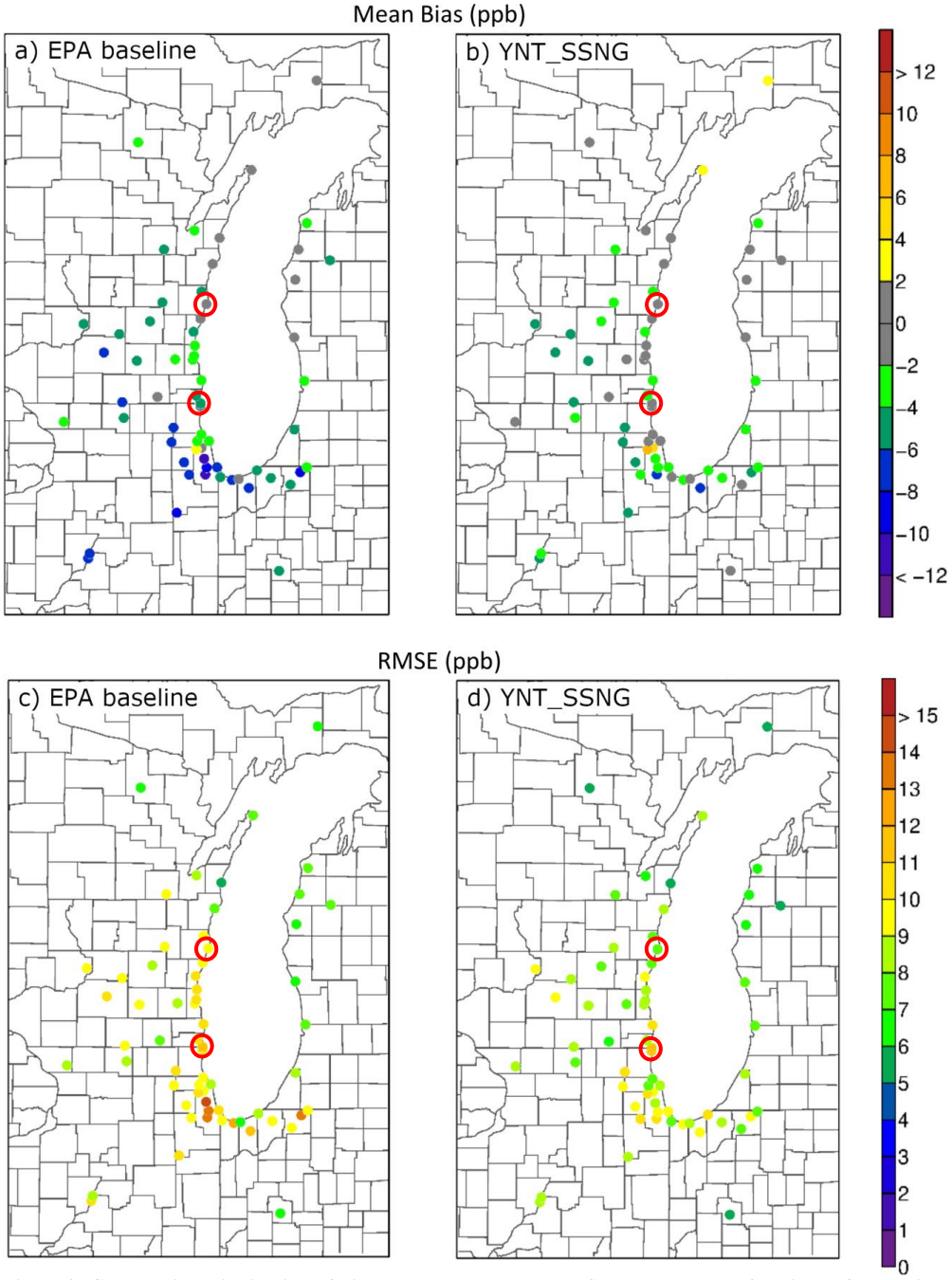

Figure 2. Geographical distribution of bias (upper panels) and RMSE (lower panels) for binned 8-h maximum ozone concentrations from the EPA (left) and YNT_SSNG (right) 1.3km CMAQ simulations using hourly data from all stations in the 1.3 km resolution inner during the LMOS period of record from 22 May 2017 to 22 June 2017. Bias and RMSE (ppbv) at each site are indicated by the color bar. Two AQS monitors, Sheboygan KA to the north and Chiwaukee Prairie along the Wisconsin-Illinois border are indicated by the red circles.

https://doi.org/10.5194/egusphere-2023-152
Preprint. Discussion started: 2 February 2023

3.1.2 Evaluation with ground-based NO_2 and HCHO measurements

During LMOS, the EPA deployed instruments measuring in-situ NO_2 and HCHO in Sheboygan, WI to characterize ozone precursors along the shore of Lake Michigan. These 1-min measurements were taken at Spaceport Sheboygan, which is approximately 9 km north of the Sheboygan, KA monitor highlighted in Figure 2. Here, we use the hourly averaged EPA NO_2 and HCHO measurements to evaluate the accuracy of prediction of ozone precursors for the YNT_SSNG and EPA CMAQ simulations.

Figures 3 and 4 show the hourly NO_2 and HCHO comparisons, respectively. There are several periods where observed NO_2 (black lines, Figure 3) is above 10 ppbv; these periods are generally underestimated by the EPA simulation and overestimated by the YNT_SSNG simulation (red lines, Figure 3). We find an overall negative bias of -0.32 ppbv for the EPA and an overall positive bias of 0.68 pbbv for the YNT_SSNG simulation. We also find that the correlations are slightly lower and RMS errors are slightly higher in the YNT_SSNG simulation than in the EPA simulation.

Observed HCHO shows peak amounts in excess of 4 ppbv (black lines, Figure 4) which are underestimated in both simulations (red lines, Figure 4). However, the YNT_SSNG simulation tends to have overall higher HCHO mixing ratios then the EPA simulation leading to a nearly 50% reduction (-0.26 versus -0.54 ppbv) in the low bias relative to the EPA measurements. This is likely due to the incorporation of more realistic (relative to climatology) GVF observations in the YNT_SSNG simulation and better representation of biogenic VOCs. Compared to the EPA simulation, we also find correlations and RMS errors are slightly lower in the YNT_SSNG simulation.

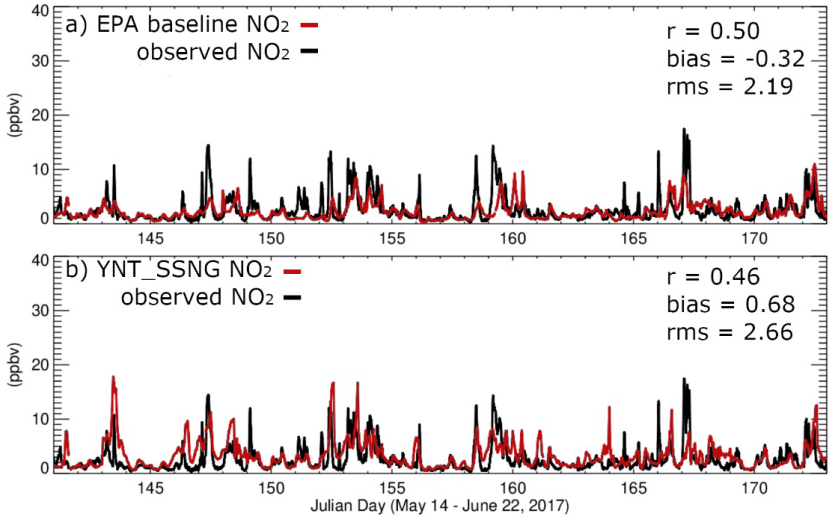

Figure 3: Timeseries of 1-hour averaged NO_2 at Spaceport Sheboygan for the 1.3km EPA (upper) and YNT_SSNG (lower) CMAQ simulations (red) and EPA observations (black) during the LMOS 2017 time period (May 22-June 21, 2017).

https://doi.org/10.5194/egusphere-2023-152
Preprint. Discussion started: 2 February 2023

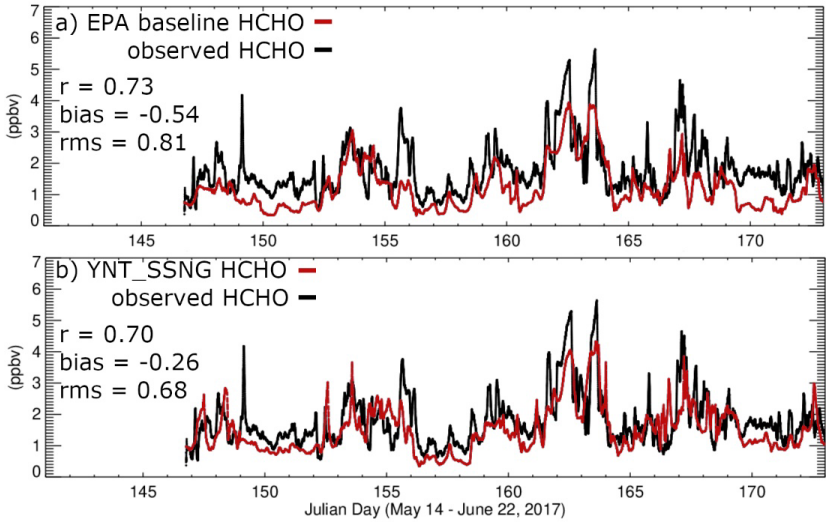

Figure 4: Timeseries of 1-hour averaged HCHO at Spaceport Sheboygan for the 1.3km EPA (upper) and YNT_SSNG (lower) CMAQ simulations (red) and EPA observations (black) during the LMOS 2017 time period (May 22-June 21, 2017).

3.2 Model performance during high-ozone events

3.2.1 Sheboygan KA and Chiwaukee Prairie 1-hour ozone

In this and the following sections, we focus on the two AQS monitors that showed high ozone events during LMOS most clearly: the Sheboygan Kolher Andrae (KA) monitor (AQS 551170006), located south of Sheboygan, WI, and the Chiwaukee Prairie monitor (AQS 550590019) is located near the Wisconsin/Illinois border. These two sites are indicated by red circles in Figure 2.

Figures 5 and 6 show the hourly AQS observed and CMAQ EPA and YNT_SSNG simulated O_3 for Sheboygan KA and Chiwaukee Prairie monitors. Comparisons with AQS observations and the two simulations at Sheboygan KA show increased correlations (0.74 versus 0.697), increased biases (1.01 versus 0.664 ppbv) and reduced RMSE (9.97 versus 10.7 ppbv) for the YNT_SSNG simulation. Similar comparisons at Chiwaukee Prairie show decreased correlations (0.64 verses 0.67), reduced biases (0.397 verses 1.44 ppbv) and increased RMSE (11.58 verses 11.12 ppbv) for the YNT_SSNG simulation. While the overall hourly ozone statistics at Sheboygan KA and Chiwaukee Prairie are relatively similar between the EPA and YNT_SSNG simulations at these sites, the simulations during high ozone events are quite different. This is illustrated by looking at composite statistics during events A, B, and C.

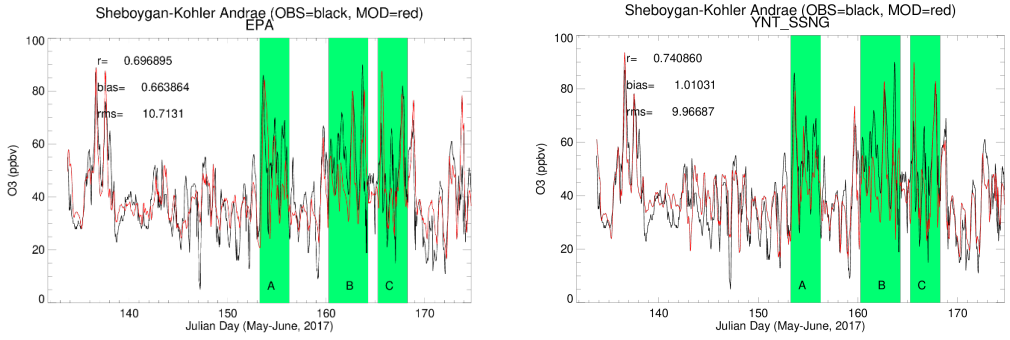

https://doi.org/10.5194/egusphere-2023-152
Preprint. Discussion started: 2 February 2023

Figure 5: Timeseries of 1-h ozone at Sheboygan-Kohler Andrae AQS monitor (551170006) for the 1.3km EPA (left) and YNT_SSNG (right) CMAQ simulations (red) and AQS observations (black) during the LMOS 2017 time period (May 22-June 21, 2017). The green highlighting shows the periods of high ozone events A, B, and C.

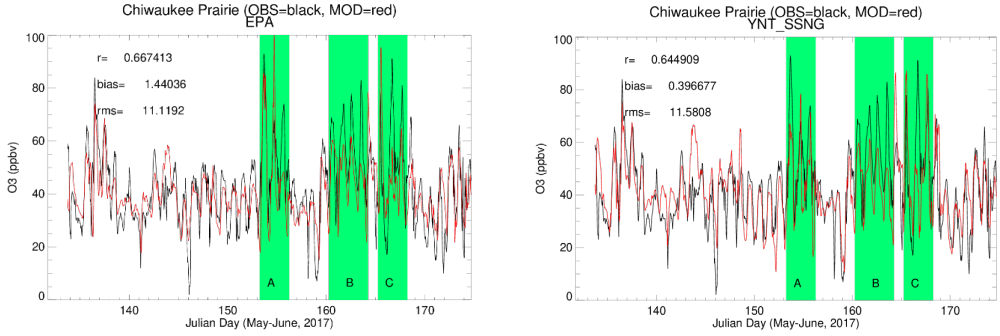

Figure 6: Same as in Figure 5 but for Chiwaukee Prairie AQS monitor (550590019).

3.2.2 Composite ozone wind roses during high ozone events A, B, C

Figure 7 shows observed and simulated composite ozone wind roses from the 1.3km EPA and YNT_SSNG simulations at the Sheboygan KA and Chiwaukee Prairie monitors during high ozone events A, B, and C. At Sheboygan KA, the observed wind direction is most frequently (>50%) from the south-southwest, which is also the direction where the majority of the higher (>60ppbv) ozone is observed during south-southeast (SSE) ozone events. The EPA simulation predicts winds which are most frequently (>30%) from the SSE with the majority of the higher ozone coming from this direction. The YNT_SSNG simulation predicts winds which are more variable but also most frequently (>20%) from the SSE with most of the higher ozone coming from this direction. The overall frequency of higher ozone in the EPA simulation (~20%) is closer to the observed percentage (~33%) than the YNT_SSNG simulation (~15%). These comparisons show that the EPA meteorology best captures the observed ozone wind rose at Sheboygan KA during high ozone events.

At Chiwaukee Prairie the observed winds are more variable and are most frequently (>40%) from the southwest. While some of the observed higher ozone comes from the southwest, the highest (> 80 ppbv) ozone comes from the SSE. Both the EPA and YNT_SSNG simulations frequently predict southwest winds (~30% and ~50%, respectively) with lower ozone (< 60 ppbv) than observed. Both the EPA and YNT_SSNG simulations show the highest ozone coming from the SSE, but the YNT_SSNG simulation more accurately captures the observed percentages of high ozone coming from the SSE while EPA simulation shows both low and high ozone coming from the southeast at Chiwaukee Prairie. The overall frequency of higher ozone in the EPA and YNT_SSNG simulations are very similar (~13%) and both underestimate the observed percentage (~35%), however, most of the higher ozone in the EPA simulation comes from the southeast. These comparisons show that the YNT_SSNG simulation best captures the observed ozone wind rose at Chiwaukee Prairie during high ozone events but that both simulations have a low bias in ozone when winds are from the southwest.

https://doi.org/10.5194/egusphere-2023-152
Preprint. Discussion started: 2 February 2023

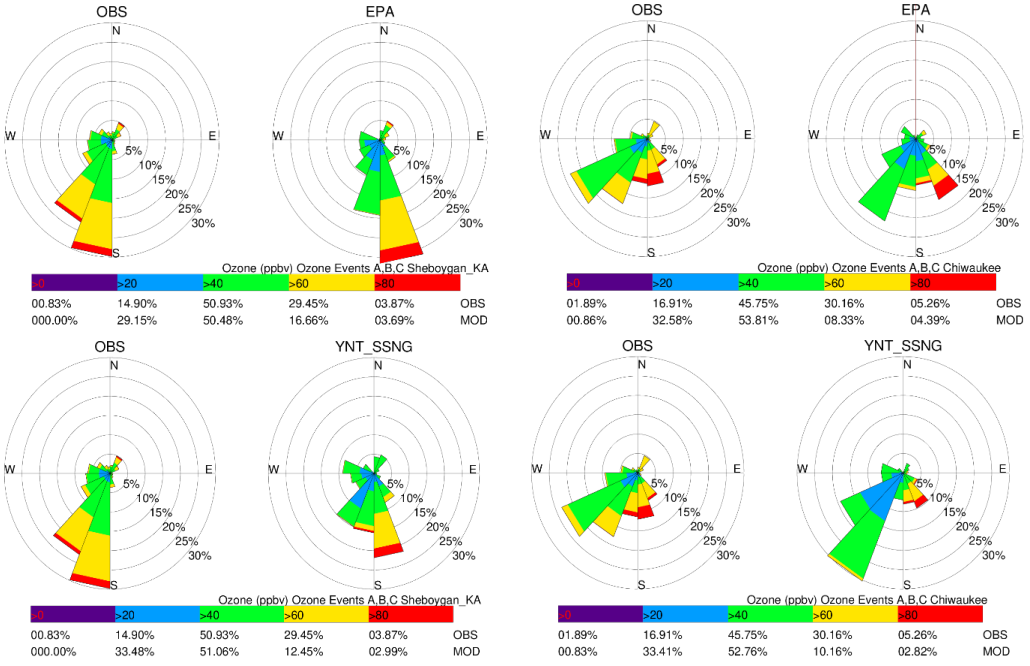

Figure 7: Observed (OBS) and simulated wind roses using 1-h ozone and wind directions at the Sheboygan-Kohler Andrae AQS monitor (551170006, left columns) and Chiwaukee Prairie AQS monitor (550590019, right columns) for the 1.3km EPA (upper rows) and YNT_SSNG (lower rows) CMAQ simulations during high ozone events A, B, and C. Wind directions are divided into 22.5 degree bins and the percentage of winds within each directional bin are indicted by the percentages on the wind rose plots. The colors within each wind direction bin indicate the distribution of observed and simulated ozone within 20ppbv bins as indicated by the color bars. The overall percentage of observed (OBS) and simulated (MOD) ozone within each ozone bin is indicated below the color bar for each site and simulation.

3.2.3 1-h ozone concentration and wind direction during high ozone events A, B, C

While the ozone wind roses presented above provide an overall comparison of the joint distribution of simulated and observed winds and ozone, they do not provide a quantitative estimate of the errors in the simulations. In this section we have binned simulated and observed ozone and wind direction to provide a more quantitative characterization of the simulated biases. Figure 8 shows bar and whisker plots of 1.3km YNT_SSNG and EPA CMAQ ozone simulations and 1-h averaged observed ozone at Chiwaukee Prairie and Sheboygan KA during high ozone events A, B, and C. Both simulations show systematic high biases for lower observed ozone concentrations (< ~40 ppbv) and low biases for higher ozone concentrations (> 50 ppbv) at both sites. These results are consistent with the 8-hour maximum ozone biases for the 1.3km domain wide comparison (Figure 1). The EPA simulation shows better agreement with observed ozone for the highest ozone (>85 ppbv) at both sites during high ozone events but shows a wider spread in the simulated distribution within each of these high observed ozone bins at Chiwaukee Prairie. The EPA and YNT_SSNG CMAQ simulations show similar distributions for observed ozone less than 80 ppbv.

https://doi.org/10.5194/egusphere-2023-152
Preprint. Discussion started: 2 February 2023

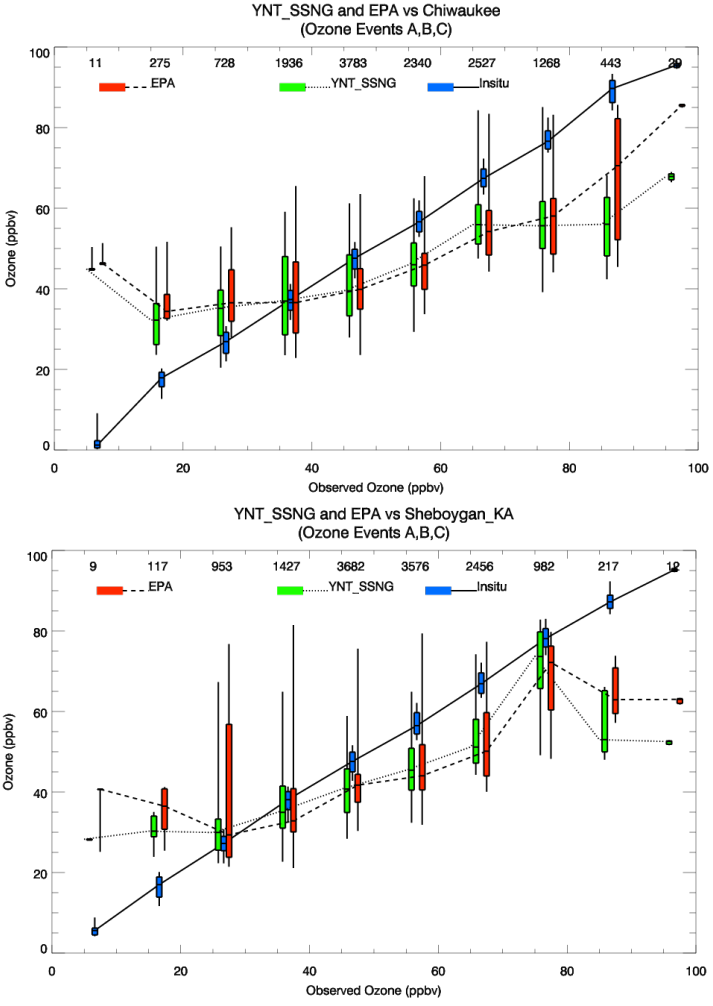

Figure 8. Bar and whisker plots showing the binned median ozone concentrations from the 1.3km EPA (dashed) and YNT_SSNG (dotted) CMAQ simulations and observed ozone (solid) at Chiwaukee Prairie (upper) and Sheboygan KA (lower) during high ozone events A, B, and C. The vertical bars show the 50% and the vertical lines show the 95% for the EPA (red) and YNT_SSNG (green) CMAQ simulations and observed ozone (blue). The total observed count within each 5 ppbv bin is indicated on the top of each panel.

Figure 9 shows bar and whisker plots of 1.3km YNT_SSNG and EPA CMAQ wind direction simulations and 1-h averaged observed wind direction at Chiwaukee Prairie and Sheboygan KA during high ozone events A, B, and C. Both simulations show a westerly bias and large variations in wind direction when the observed winds have an easterly component (0-180º) at Chiwaukee Prairie. Winds with an easterly component account for 30% of the observed wind directions at this site. Both simulations show a systematic easterly bias in wind direction when the observed winds have a westerly component (180-360º) at both sites, but the YNT_SSNG simulation is in better agreement with observations when the wind is from the southwest, west, and northwest(240-290º). The two simulations show small (~20º) easterly biases when the observed winds are from the prevailing wind direction at Chiwaukee (south to west-southwest, 180-260º) and Sheboygan (south to south-southwest, 180-220º) which account for 61% and 54% of the observed wind directions, respectively. The YNT_SSNG simulation shows the smallest (~10º) easterly biases during prevailing winds at Chiwaukee.

https://doi.org/10.5194/egusphere-2023-152
Preprint. Discussion started: 2 February 2023

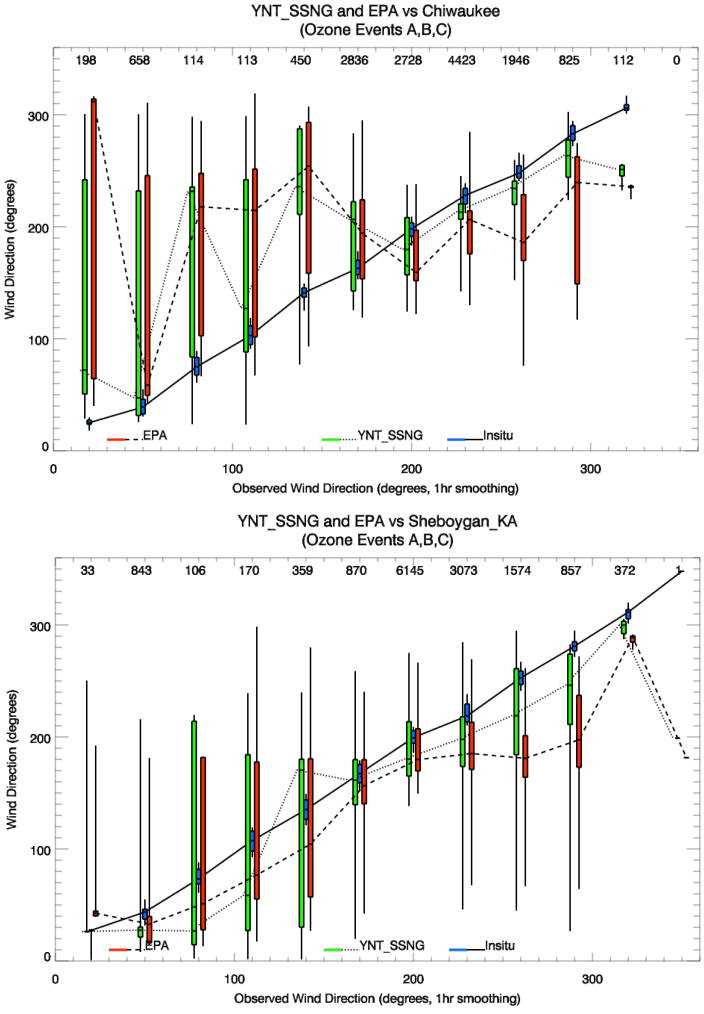

Figure 9. Bar and whisker plots showing the binned median wind direction from the 1.3km EPA (dashed) and YNT_SSNG (dotted) CMAQ simulations and observed wind direction (solid) at Chiwaukee Prairie (upper) and Sheboygan KA (lower) during high ozone events A, B, and C. The vertical bars show the 50% and the vertical lines show the 95% for the EPA (red) and YNT_SSNG (green) CMAQ simulations and 1-hour averaged observed wind direction (blue). The total observed count within each 20° bin is indicated on the top of the figures.

3.2.4 GEOTASO comparisons during high ozone events A, B, C

Here, we use GeoTASO (Nowlan et al., 2016) NO_2 and HCHO column measurements to verify ozone precursors within the YNT_SSNG and EPA simulations during high ozone events A, B, and C. Figure 10 shows the results of the NO_2 column analysis. Compared to observed NO_2 column measurements, the YNT_SSNG and EPA simulations have similar correlation (0.60 vs. 0.57) and the YNT_SSNG has a substantially reduced bias (0.17×10^{15} vs. 0.35×10^{15} mol/cm^2), although still within the uncertainty of the GeoTASO measurements. Figure 11 shows the results of the HCHO column analysis. Compared to observed HCHO column measurements, the YNT_SSNG has a lower correlation than the EPA simulation (0.24 vs. 0.31) and a larger bias (3.0×10^{15} vs. 1.8×10^{15} mol/cm^2).

Nowlan et al. (2018) used comparisons between the GEOstationary Coastal and Air Pollution Events (GEO-CAPE) Airborne Simulator (GCAS, which is similar to the GeoTASO instrument) NO_2 and HCHO retrievals and columns

https://doi.org/10.5194/egusphere-2023-152
Preprint. Discussion started: 2 February 2023

estimated from airborne in-situ NO_2 and HCHO profiles to estimate mean precisions of 1 x 10^{15} mol/cm^2 and 19 x 10^{15} mol/cm^2 for the native (250m) resolution NO_2 and HCHO retrievals, respectively. The LMOS 2017 GeoTASO radiances were co-added onto a 1km grid during the 2017 LMOS campaign so we anticipate that the precision of the 1km retrievals are better by a factor of 2. Given the relatively high precision of GeoTASO NO_2 compared to the column amounts observed during high ozone events A, B and C, we conclude that the high bias in NO_2 columns in the EPA simulation is meaningful. We have less confidence in the significance of the differences between the YNT_SSNG and EPA HCHO columns relative to the GeoTASO retrievals since the observed HCHO columns are on the order of the precision of the instrument and the biases in column HCHO measurements are less than the GeoTASO precision during high ozone events A, B, and C. Our results show the YNT_SSNG simulation has an improved representation NO_2, which is a primary ozone precursor, during these high ozone events.

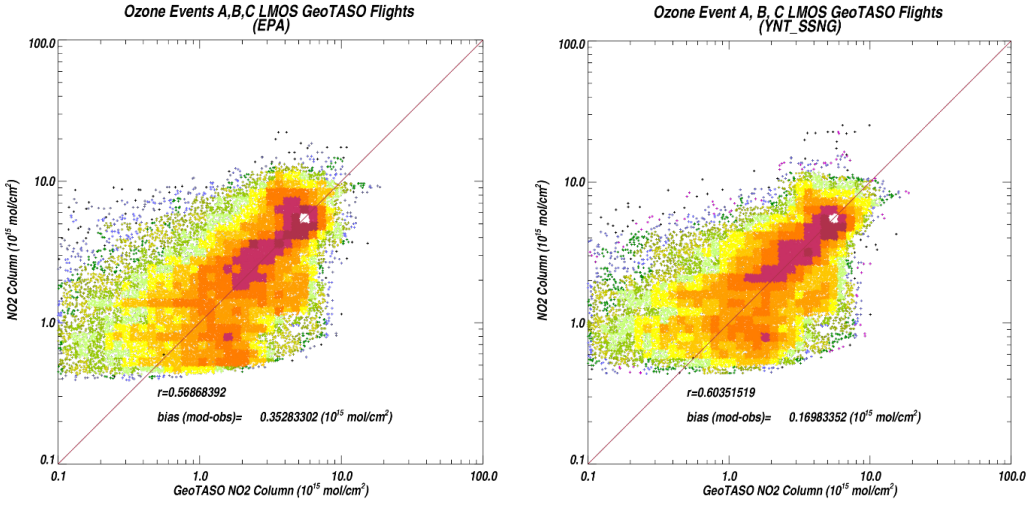

Figure 10. Scatter plots of 1.3km EPA (left) and YNT_SSNG (right) NO_2 columns verses GEOTASO NO_2 columns (x 10^{15} mol/cm^2) during LMOS 2017 high ozone events A, B, and C.

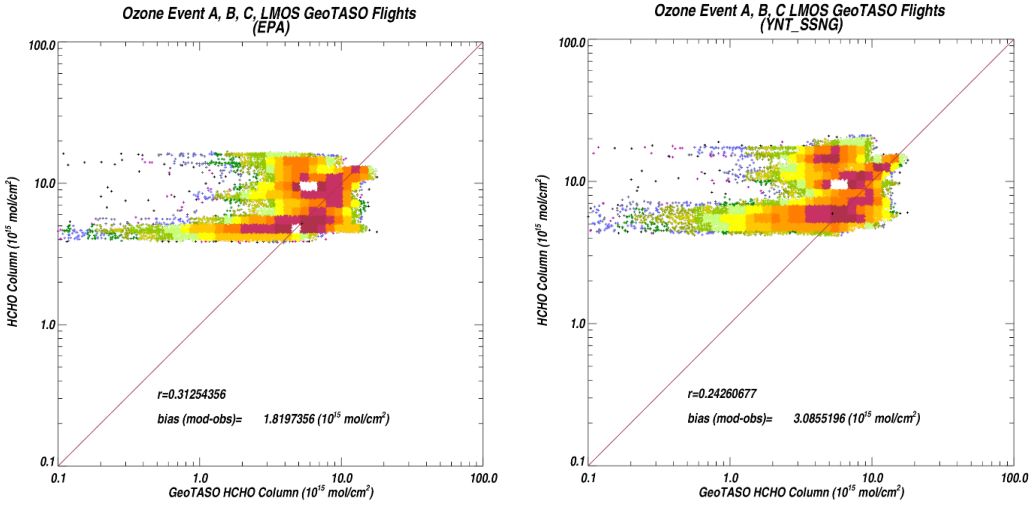

Figure 11. Same as in Figure 10 but for HCHO columns.

https://doi.org/10.5194/egusphere-2023-152
Preprint. Discussion started: 2 February 2023

3.3 June 2, 2017 ozone exceedance event

The only ozone exceedance event that had significant inland penetration of the lake breeze at both Chiwaukee and Sheboygan KA during LMOS 2017 occurred on June 2nd, 2017 (Stanier et al, 2021; Wagner et al, 2022). The simulations on this day most clearly illustrates the differences between the EPA and YNT_SSNG results. Figure 12 shows the observed visible (0.64 micron) reflectance from the Advanced Baseline Imager (ABI) on the NOAA GOES-16 satellite and surface ozone concentrations from the YNT_SSNG and EPA simulations, respectively, at 22 UTC (5pm CDT) on June 2, 2017. To delineate the simulated continental convective and stable maritime boundary layers we also show where the YNT_SSNG and EPA simulated PBL heights are >1 km (Figure 12, Red or Green lines in the ABI panel). These contours roughly correspond to the western most edge of the simulated marine boundary layer and indicate the extent of the penetration of the lake breeze circulation. The ABI visible reflectances clearly show where the stable marine boundary layer suppresses the formation of fair-weather cumulus clouds, which form within the turbulent continental boundary layer and are evident to the west of the YNT_SSNG 1-km PBL height contour. The YNT_SSNG simulation shows a more extensive penetration of high ozone concentrations inland, in agreement with the extent of the penetration of the marine boundary layer. In contrast, the EPA simulation shows very little penetration of the stable marine boundary layer. This lake breeze penetration has a significant impact on the simulated surface ozone distributions with deeper penetration of high ozone inland.

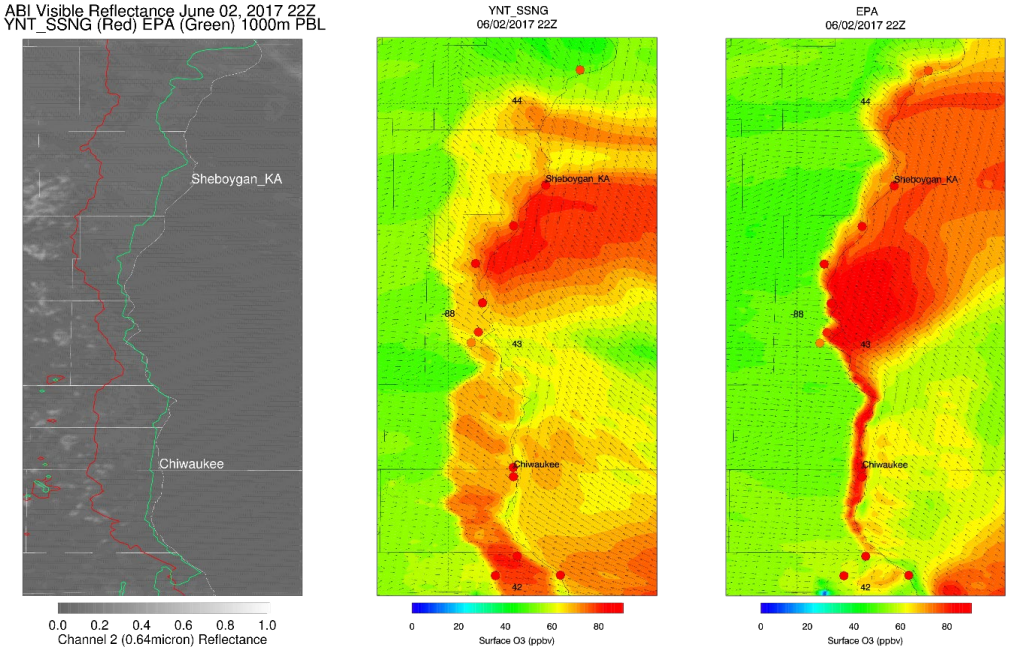

Figure 12: ABI visible (0.64micron) reflectance (left), YNT_SSNG surface ozone (ppbv, middle), and EPA surface ozone (ppbv, right) at 22 UTC on June 2, 2017. Observed AQS ozone concentrations at 22 UTC are shown as colored circles. Location of 1km YNT_SSNG (Red) and EPA (Green) PBL heights are also shown in the ABI (left) panel. The locations of the Shebogan, KA and Chiwaukee Prairie AQS monitors are labeled in each of the panels.

Figure 13 shows comparisons between airborne GeoTASO, YNT_SSNG, and EPA column NO_2 along the western shore of Lake Michigan on June 2, 2017. Comparisons with column NO_2 distributions provide a means of comparing the fidelity of the lake breeze transport of ozone precursors during this high ozone event. Observed NO_2 columns peak near 10 x 10^{15}mol/cm^2 and shows penetration of the high NO_2 column amounts inland by the lake breeze circulation, consistent with the ABI visible reflectances. The GeoTASO NO_2 columns show peak amounts of 10x10^{15} mol/cm^2 and significant inland penetration of higher NO_2 columns over the southern portion of the flight track. The YNT_SSNG NO_2 column shows similar peak amounts and shows similar, but not as far inland, penetration of the high NO_2 columns. The EPA NO_2 column shows localized NO_2 columns over 15 x 10^{15} mol/cm^2 along the Lake Michigan

https://doi.org/10.5194/egusphere-2023-152
Preprint. Discussion started: 2 February 2023

shoreline and does not predict as much onshore penetration. The narrow plume of higher GeoTASO NO_2 column extending to the northwest from the coast north of the Sheboygan KA AQS monitor is a signature of the Edgewater coal-fired power plant. The YNT_SSNG and EPA simulations also show this plume, but the YNT_SSNG simulation does a better job of capturing the northwestward transport of the plume while the EPA simulation shows transport of this narrow plume to the north-northeast.

Figure 14 shows comparisons between airborne GeoTASO, YNT_SSNG, and EPA column HCHO along the western shore of Lake Michigan on June 2, 2017. HCHO columns vary much less spatially than NO2 columns given that the former is formed through VOC oxidation while the latter is primarily associated with emissions. Both simulations capture the observed north-to-south positive gradient providing some confidence in the larger scale gradients. However, the GeoTASO HCHO measurements show values in excess of $10x10^{15}$ mol/cm^2 over Lake Michigan that are not captured in either the YNT_SSNG or EPA HCHO column simulations. Given the lower precision GeoTASO HCHO columns, the differences between the YNT_SSNG and EPA HCHO columns are difficult to quantify with these measurements. We note large differences between simulated and observed GeoTASO NO_2 and HCHO over the eastern portion of observations. These observations were collected later during the flight and therefore subject to larger uncertainties related to the impact of stratospheric NO2 and ozone absorption interferences resulting in a drift in the baseline measurements.

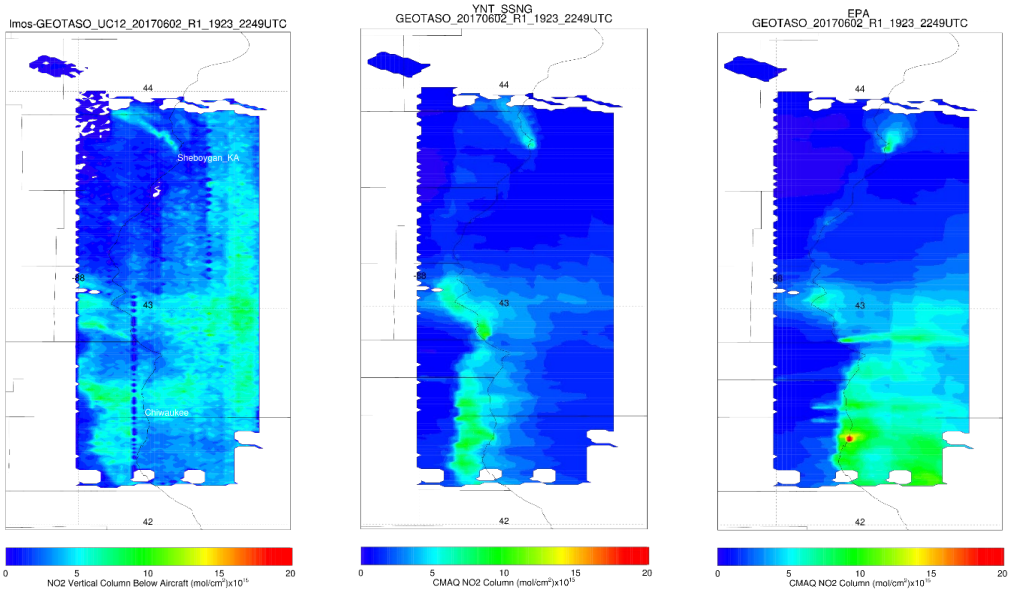

Figure 13: GEOTASO (left), YNT_SSNG (middle), and EPA (right) Column NO_2 (x 10^{15} mol/cm^2) on June 2, 2017. The location of the Sheboygan, KA AQS station is labeled in the GEOTASO column NO_2 panel.

https://doi.org/10.5194/egusphere-2023-152
Preprint. Discussion started: 2 February 2023

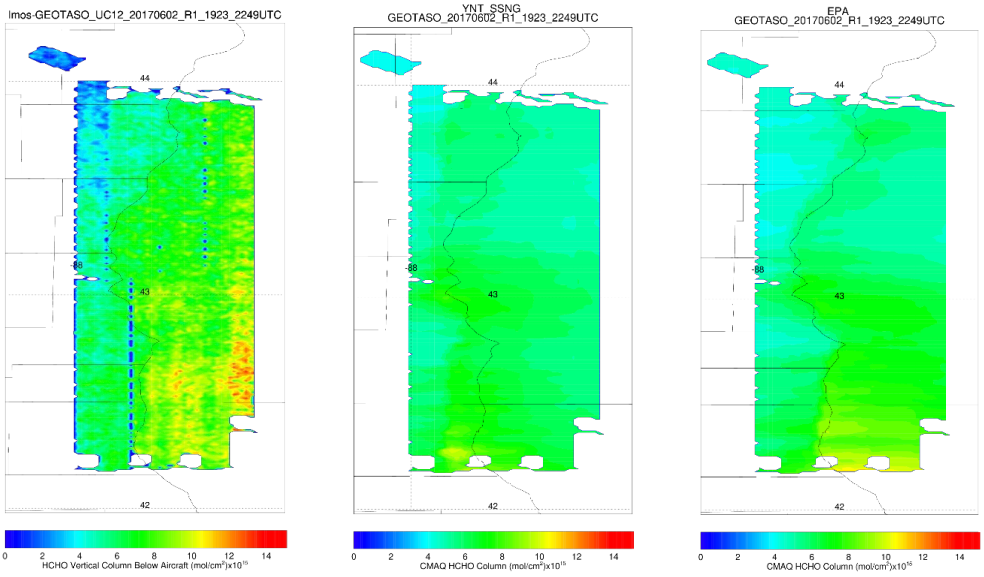

Figure 14: GEOTASO (left), YNT_SSNG (middle), and EPA (right) Column HCHO (x 10^{15}mol/cm^2) on June 2, 2017.

Figure 15 shows comparisons between observed time height cross-sections of thermodynamic (temperature) and kinematic (wind) distributions at Sheboygan WI during the June 02, 2017 ozone exceedance event. Observed temperatures are obtained from the UW-Madison Atmospheric Emitted Radiance Interferometer (AERI) instrument (Knutson et al, 2004a,b) while wind direction and speed are obtained from a Halo Photonics doppler wind lidar instrument. Both of these instruments were deployed at the Sheboygan, WI ground site during LMOS 2017 (Stanier et al, 2021; Wagner et al, 2022). AERI temperatures show a well-defined nocturnal boundary layer with a thin layer of cold temperatures below 100-m AGL and a warmer layer extending up to approximately 600 m. The continental convective boundary layer begins to form as the sun rises (~12Z [7am CDT]). This is evident in the warmer surface temperatures near 15 UTC (10am CDT). The AERI measurements show a new shallow layer of cooler air below 50m arriving at 17 UTC (12pm CDT) associated with the stable marine boundary layer. Observed wind directions are out of the NW prior to 15 UTC at 7m/s, rapidly diminish around 15 UTC, and switch to the SE around 18 UTC (1pm CDT) when the lake breeze reaches Sheboygan, WI. The YNT_SSNG simulation captures the thermal structure of the nocturnal boundary layer and timing of the maritime boundary layer but underestimates the surface temperatures within the convective boundary layer. The YNT_SSNG simulation captures the vertical structure of the lake breeze wind speed and direction, but the timing of the switch in wind direction is about 3 hours too early. In contrast, the EPA simulation shows no thermodynamic signature of a nocturnal or marine boundary layer and underestimates the sharp change in the observed windspeed and direction.

https://doi.org/10.5194/egusphere-2023-152
Preprint. Discussion started: 2 February 2023

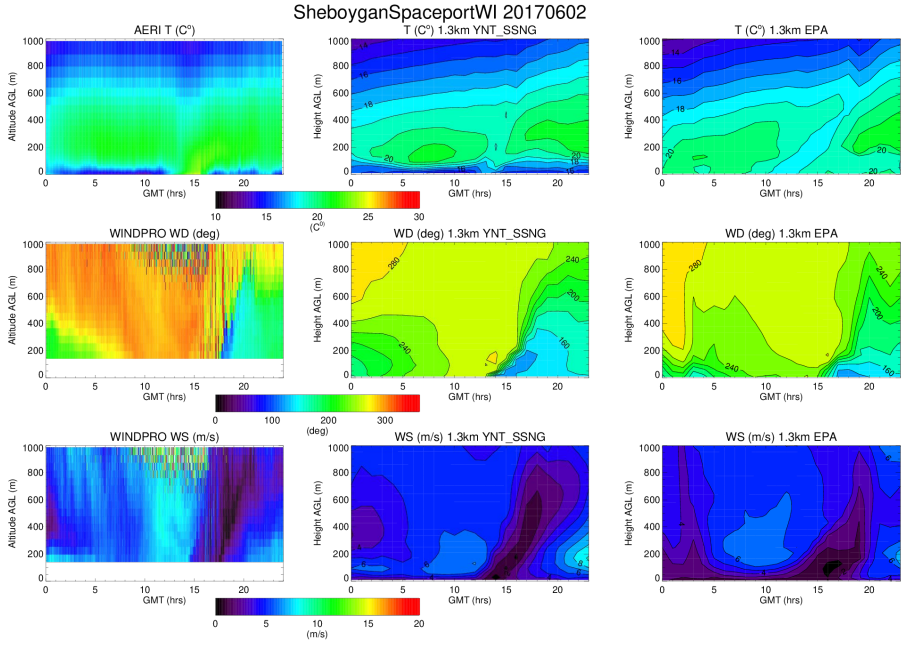

Figure 15: Time height curtains of observed (left column), YNT_SSNG (middle column), and EPA (right column) temperature (T, C°, upper row), wind direction (WD, degrees, middle row), and wind speed (WS, m/s, lower row) at Sheboygan WI on June 2, 2017. Observed temperature is from UW-Madison AERI and observed winds are from the Halo Photonics doppler wind lidar instrument.

4. Discussion and Conclusions

We have conducted an evaluation of two model simulations employing differing meteorological inputs, with the goal of identifying a model configuration best suited for characterizing the spatial and temporal variability of ozone and its precursors where lake breezes commonly affect local air quality along the Lake Michigan shoreline. We focus on the period of the LMOS campaign, 22 May – 22 June 2017, using the innermost grid of a triple-nested simulation around Lake Michigan, with a horizontal resolution of 1.3 km. The EPA simulation used best-practice recommendations (Personal communication, Jon Pleim and Robert Gilliam US EPA) for WRF inputs to the CMAQ model, including nudging to observed near-surface conditions; our YNT_SSNG simulation used different WRF parameterizations, as well as constraints to satellite observations of green vegetation fraction and soil temperature and moisture, as detailed by Otkin et al. (2022).

Both model simulations reasonably capture observed daily maximum 8-h average ozone amounts over the study period, however both simulations underestimating ozone amounts at times with high ozone and overestimating ozone when observations were lower. Both model simulations also perform similarly on an hourly basis on high ozone days. We find the EPA simulation better represents hourly ozone when observed amounts are high (80-90 ppbv), and the YNT_SSNG simulation overall biases are generally smaller (less negative) than those of the EPA simulation. Both simulations also tend to underestimate amounts of the ozone precursor HCHO, with smaller (less negative) biases in the YNT_SSNG simulation likely resulting from the incorporation of satellite-derived GVF and therefore more realistic in-line calculations of biogenic VOC emissions. We find the simulations are less similar in their representation of NO_2 amounts; while the EPA simulation tends to underestimate NO_2 at monitor sites, the YNT_SSNG simulation has an overall high (positive) bias.

https://doi.org/10.5194/egusphere-2023-152
Preprint. Discussion started: 2 February 2023

Since the simulations use identical emissions and chemistry, the differences in modeled ozone and precursors are linked to the differences in both horizontal and vertical transport. In Part 1 of this study, Otkin et al. (2022) noted the EPA simulation had an overall low bias in wind speed, the YNT_SSNG simulation had a positive bias, and the simulations had similar RMSE. Here, we find many similarities between simulations on high ozone days. At Chiwaukee Prairie, we find both simulations capture the highest ozone amounts transported from the SSE. On high ozone days at Sheboygan KA, observed winds tend to be SSW, while both models show highest ozone amounts transported from the SSE. At both locations, both simulations tend to have a westerly bias when observed winds have an easterly (onshore) component.

We find greater differences in column amounts of ozone precursors. The EPA simulation has a negative bias in near-surface NO_2, a positive bias in column NO_2 amounts, and elevated column amounts concentrated along the Lake Michigan shoreline during the ozone exceedance event on June 2nd. The YNT_SSNG simulation has a small positive bias in NO_2 column amounts, with elevated column amounts extending further inland on the lake-breeze enhanced ozone event on June 2nd. While these differences reflect the parameterizations used to generate input meteorology, differences in vertical mixing, and ensuing column amounts of NO_2 and HCHO discussed here, are further complicated by CMAQ using the ACM2 parameterization for vertical diffusion—a mismatch for the YNT_SSNG simulation that influences our evaluation since it leads to differences in boundary layer mixing. Still, the NO_2 column comparisons provide support for the improved representation of lake breeze transport of ozone precursors in the YNT_SSNG simulation. Future model comparisons with upcoming geostationary observations will allow for maturing analysis for assessing model performance with respect to the diurnal evolution of precursors during ozone events.

Our thermodynamic and kinematic comparison of the EPA and YNT_SSNG simulations show improved representation of not only the extent, but of the timing of the lake breeze in the YNT_SSNG simulation. This is consistent with the meteorological analysis presented in Part 1 of this study, where the YNT_SSNG had a better representation of diurnal patterns (Otkin et al., 2022). However, we note that the meteorological inputs to our simulations are hourly, as is typically used in air quality modeling studies. Both simulations would likely benefit from sub-hourly winds given the rapid changes that can occur in the presence of lake and land breeze circulations. For this, a two-way, coupled model such as WRF-CMAQ (Wang et al., 2021) would be better suited for a goal of better simulating the fine temporal and spatial scales of lake breeze transport and chemistry.

This analysis complements other studies in evaluating the impact of changing meteorological inputs and parameterizations on air quality in a complex environment. Appel et al. (2014) also found improved representation of ozone in environments with bay and sea breezes with the addition of high-resolution SST into the WRF and CMAQ modeling framework. Cheng et al. (2012) underscored the importance of PBL parameterization in simulating land-sea breezes and their impacts on near-surface ozone. Similar to our work, Banks and Baldasano (2016) evaluated the impacts of PBL parameterizations on air quality and also found ambiguous results, with the simulation using the YSU PBL better capturing observed NO_2, and the simulation using the ACM2 PBL better capturing observed ozone. Future work will be able to take advantage of ongoing improvements to both WRF and CMAQ, such as an update to the calculation of vegetative fraction and PX-LSM soil parameters in WRF (Appel et al., 2021), and should explore the relationships among spatial and temporal resolution of meteorological parameterizations themselves along with those of the modeling framework.

Acknowledgments

Funding for this project was provided by the NASA Health and Air Quality (HAQ) program via grant #80NSSC18K1593. We wish to thank the 2017 Lake Michigan Ozone Study Instrument teams for the GeoTASO, AERI, Doppler Wind Lidar, and surface measurements used in this study. We also wish to thank Laura Judd and Scott Janz for their review of the manuscript.

References

Abdi-Oskouei, M., G. Carmichael, M. Christiansen, G. Ferrada, B. Roozitalab, N. Sobhani, K. Wade, A. Czarnetzki, R. B. Pierce, T. Wagner, and C. Stanier (2020), Sensitivity of Meteorological Skill to Selection of WRF-Chem Physical Parameterizations and Impact on Ozone Prediction During the Lake Michigan Ozone Study (LMOS), *J. Geophys. Res. Atmos., 125*(5), doi:10.1029/2019JD031971.

Adams, E. (2020), 2017 v1 NEI Emissions Modeling Platform (Premerged CMAQ-ready Emissions), doi:10.15139/S3/TCR6BB, UNC Dataverse, V1.

https://doi.org/10.5194/egusphere-2023-152
Preprint. Discussion started: 2 February 2023

Adelman, Z. (2020), LADCO public issues, https://www.ladco.org/public-issues/

Appel, K. W., R. C. Gilliam, J. E. Pleim, G. Pouliot, D. C. Wong, S. J. Roselle, and R. Mathur (2014), Improvements to the WRF-CMAQ modeling system for fine-scale air quality applications to the DISCOVER-AQ Baltimore/Washington D.C. campaign. *EM: Air and Waste Management Associations Magazine for Environmental Managers. Air & Waste Management Association*, September 2014 Issue, 16-21.

Appel, K. W., J. O. Bash, K. M. Fahey, K. M. Foley, R. C. Gilliam, C. Hogrefe, W. T. Hutzell, D. Kang, R. Mathur, B. N. Murphy, S. L. Napelenok, C. G. Nolte, J. E. Pleim, G. A. Pouliot, H. O. T. Pye, L. Ran, S. J. Roselle, G. Sarwar, D. B. Schwede, F. I. Sidi, T. L. Spero, and D. C. Wong (2021), The Community Multiscale Air Quality (CMAQ) model versions 5.3 and 5.3.1: system updates and evaluation, *Geosci. Model Dev., 14*, 2867-2897, doi: 10.5194/gmd-14-2867-2021

Banks, B. F., and J. M. Baldasano (2016), Impact of WRF model PBL schemes on air quality simulations over Catalonia, Spain, *Sci. Total Environ., 572*, 98-113, doi: 10.1016/j.scitotenv.2016.07.167

Byun, D., and K. L. Schere (2006), Review of the governing equations, computational algorithms, and other components of the Models-3 Community Multiscale Air Quality (CMAQ) modeling, *Appl. Mech. Rev.*, *59*(1–6), 51–77, doi:10.1115/1.2128636.

Carlton, A. G., and K. R. Baker (2011), Photochemical modeling of the Ozark isoprene volcano: MEGAN, BEIS, and their impacts on air quality predictions, *Environ. Sci. Technol.*, *45*(10), 4438–45, doi:10.1021/es200050x.

Case, J. L. (2016), From drought to flooding in less than a week over South Carolina, *Results Phys., 6*, 1183-1184, doi:10.1016/j.rinp/2016.11.012.

Case, J. L., and B. T. Zavodsky (2018), Evolution of drought in the southeastern United States from a land surface modeling perspective, *Results Phys., 8*, 654-656, doi:10.1016/j.rinp.2017.12.029.

Chen, F., and J. Dudhia (2001), Coupling an advanced land-surface/hydrology model with the Penn State/NCAR MM5 modeling system. Part I: Model description and implementation, *Mon. Wea. Rev., 129*(4), 569-585, doi:10.1175/1520-0493(2001)129<0569:CAALSH>2.0.CO;2.

Cheng, F.-Y., S.-C. Chin, and T.-H. Liu (2012), The role of boundary layer schemes in meteorological and air quality simulations of the Taiwan area, *Atmos. Env., 54*, 714-727, doi: 10.1016/j.atmosenv.2012.01.029

Cleary, P. A., A. Dickens, M. McIlquham, M. Sanchez, K. Geib, C. Hedberg, J. Hupy, M. W. Watson, M. Fuoco, E. R. Olson, R. B. Pierce, C. Stanier, R. Long, L. Valin, S. Conley, and M. Smith (2021), Impacts of lake breeze meteorology on ozone gradient observations along Lake Michigan shorelines in Wisconsin, *Atmos. Env., 269*, 118834, doi:10.1016/j.atmosenv.2021.118834.

Clifton, O. E., D. L. Lombardozzi, A. M. Fiore, F. Paulot, and L. W. Horowitz (2020), Stomatal conductance influences interannual variability and long-term changes in regional cumulative plant uptake of ozone, *Env. Res. Lett., 15*(11), 114059, doi:10.1088/1748-9326/abc3f1.

Daggett, D. A., J. D. Myers, and H. A. Anderson (2000), Ozone and particulate matter air pollution in Wisconsin: trends and estimates of health effects, *Wis. Med. J., 99*(8), 47-51.

Di, Q., Y. Wang, A. Zanobetti, Y. Wang, P. Koutrakis, C. Choirat, F. Dominici, and J. D. Schwartz (2017), Air Pollution and Mortality in the Medicare Population, *N. Engl. J. Med., 376*, 2513-2522, doi:10.1056/NEJMoa1702747.

Dye, T. S., P. T. Roberts, and M. E. Korc (1995), Observations of Transport Processes for Ozone and Ozone Precursors during the 1991 Lake Michigan Ozone Study, J. Appl. Metrorol. Climatol., 34(8), 1877-1889, doi:10.1175/1520-0450(1995)034<1877:OOTPFO>2.0.CO;2.

Ek, M. B., K. E. Mitchell, Y. Lin, E. Rogers, P. Grunmann, V. Koren, G. Gayno, and J. D. Tarpley (2003), Implementation of Noah land surface model advances in the National Centers for Environmental Prediction operational mesoscale Eta model, *J. Geophys. Res., 108*(D22), 8851, doi:10.1029/2002JD003296.

Emery, C., J. Jung, B. Koo, and G. Yarwood (2015), *Improvements to CAMx Snow Cover Treatments and Carbon Bond Chemical Mechanism for Winter Ozone. Final Report*, prepared for Utah Department of Environmental Quality, prepared by Ramboll Environ, Novato, CA.

Fast, J. D., and W. E. Heilman (2003), The Effect of Lake Temperatures and Emissions on Ozone Exposure in the Western Great Lakes Region, *J. Appl. Meteorol. Climatol., 42*(9), 1197-1217, doi:10.1175/1520-0450(2003)042<1197:TEOLTA>2.0.CO;2.

Foley, T., E. A. Betterton, P. E. R. Jacko, and J. Hillery (2011), Lake Michigan air quality: The 1994-2003 LADCO Aircraft Project (LAP), *Atmos. Env., 45*(18), 3192-3202, doi:10.1016/j.atmosenv.2011.02.033.

Gilliam, R. C., and J. E. Pleim (2010), Performance assessment of new land surface and planetary boundary layer physics in the WRF-ARW, *J. Appl. Meteorol. Climatol., 49*(4), 760-774, doi: 10.1175/2009JAMC2126.1.

Guenther, A., C. N. Hewitt, D. Erickson, R. Fall, C. Geron, T. Graedel, P. Harley, L. Klinger, M. Lerdau, W. A. McKay, T. Pierce, B. Scholes, R. Steinbrecher, R. Tallamraju, J. Taylor, and P. Zimmerman (1995), A global

https://doi.org/10.5194/egusphere-2023-152
Preprint. Discussion started: 2 February 2023

model of natural volatile organic compound emissions, *J. Geophys. Res., 100*(D5), 8873-8892, doi: 10.1029/94JD02950.

Hall, S. J., P. A. Matson, and P. M. Roth (1996), NOx emissions from soil: Implications for air quality modeling in agricultural regions, *Annu. Rev. Energy Environ., 21*(1), 311-346, doi: 10.1146/annurev.energy.21.1.311

He, C., J. Cheng, X. Zhang, M. Douthwaite, S. Pattison, and Z. P. Hao (2019), Recent advances in the catalytic oxidation of volatile organic compounds: A review based on pollutant sorts and sources, *Chem. Rev., 119*(7), 4471-4568, doi:10.1021/acs.chemrev.8b00408.

Hong, S.-Y., Y. Noh, and J. Dudhia (2006), A new vertical diffusion package with explicit treatment of entrainment processes, *Mon. Wea. Rev., 134*(9), 2318-2341, doi:10.1175/MWR3199.1.

Iacono, M. J., J. S. Delamere, E. J. Mlawer, M. W. Shephard, S. A. Clough, and W. D. Collins (2008), Radiative forcing by long-lived greenhouse gases: Calculations with the AER radiative transfer models, *J. Geophys. Res., 113*(D13), doi:10.1029/2008JD009944.

Judd, L. A., J. A. Al-Saadi, S. J. Janz, M. G. Kowalewski, R. B. Pierce, J. J. Szykman, L. C. Valin, R. Swap, A. Cede, M. Mueller, M. Tidfengraber, N. Abuhassan, and D. Williams (2019), Evaluating the impact of spatial resolution on tropospheric NO2 column comparisons within urban areas using high-resolution airborne data, *Atmos. Meas. Tech., 12*(11), 6091-6111, doi: 10.5194/amt-12-6091-2019.

Juncosa Calahorrano, J. F., J. Lindaas, K. O'Dell, B. B. Palm, Q. Peng, F. Flocke, I. B. Pollack, L. A. Garofalo, D. K. Farmer, J. R. Pierce, J. L. Collett Jr., A. Weinheimer, T. Campos, R. S. Hornbrook, S. R. Hall, K. Ullmann, M. A. Pothier, E. C. Apel, W. Permar, L. Hu, A. J. Hills, D. Montzka, G. Tyndall, J. A. Thornton, and E. V. Fischer (2020), Daytime oxidized reactive nitrogen portioning in Western U.S. wildfire smoke plumes, J. Geophys. Res. Atmos., 126(4), doi:10.1029/2020JD033484.

Kain, J. S. (2004), The Kain-Fritsch convective parameterization: An update, *J. Appl. Meteorol. Climatol., 43*(1), 170-181, doi:10.1175/1520-0450(2004)043<0170:TKCPAU>2.0.CO;2.

Knuteson, R. O., and Coauthors, 2004a: Atmospheric emitted radiance interferometer. Part I: Instrument design. J. Atmos. Oceanic Technol., 21, 1763–1776, https://doi.org/10.1175/JTECH-1662.1.

Knuteson, R. O,, and Coauthors, 2004b: Atmospheric emitted radiance interferometer. Part II: Instrument performance. J. Atmos. Oceanic Technol., 21, 1777–1789, https://doi.org/10.1175/JTECH-1663.1.

Lamsal, L. N., R. V. Martin, A. van Donkelaar, E. A. Celarier, E. J. Bucsela, K. F. Boersma, R. Dirksen, C. Luo, and Y. Wang (2010), Indirect validation of tropospheric nitrogen dioxide retrieved from the OMI satellite instrument: Insight into the seasonal variation of nitrogen oxides at northern midlatitudes, *J. Geophys. Res. Atmos., 115*(D5), doi:10.1029/2009JD013351.

Lawrence, M. G., and P. J. Crutzen (1999), Influence of NOx emissions from ships on tropospheric photochemistry and climate, *Nature, 402*, 167-170, doi: 10.1038/46013.

Leitch, J. W., T. Delker, W. Good, L. Ruppert, F. Murcray, K. Chance, X. Liu, C. Nowlan, S. Janz, N. A. Krotkov, K. E. Pickering, M. Kowalewski, and J. Wang (2014), The GeoTASO airborne spectrometer project, *Proc. SPIE 9218, Earth Observing Systems XIX,* 17-21 August 2014, San Diego, doi: 10.1117/12.2063763.

Lelieveld, J., J. S. Evans, M. Fnais, D. Giannadaki, and A. Pozzer (2015), The contribution of outdoor air pollution to premature mortality on the global scale, *Nature, 525*(7569), 367-371, doi:10.1038/nature15371

Lennartson, G. J., and M. D. Schwartz (2002), The lake breeze--ground-level ozone connection in eastern Wisconsin: a climatological perspective, *Int. J. Climatol., 22*(11), 1347-1364, doi:10.1002/joc.802.

Luecken, D. J., G. Yarwood, and W. T. Hutzell (2019), Multipollutant modeling of ozone, reactive nitrogen and HAPs across the continental US with CMAQ-CB6, *Atmos. Environ.*, *201*(July), 62–72, doi:10.1016/j.atmosenv.2018.11.060.

Manisalidis, I., E. Stavropoulou, A. Stavropoulos, E. Bezirtzoglou (2020), Environmental and Health Impacts of Air Pollution: A Review, *Front. Public Health, 8*(14), doi: 10.3389/fpubh.2020.00014

Mlawer, E. J., S. J. Taubman, P. D. Brown, M. J. Iacono, and S. A. Clough (1997), Radiative transfer for inhomogeneous atmospheres: RRTM, a validated correlated-k model for the longwave, *J. Geophys. Res., 102*(D14), 16663-16682, doi:10.1029/97JD00237.

Nowlan, C. R., et al (2016), Nitrogen dioxide observations from the Geostationary Trace gas and Aerosol Sensor Optimization (GeoTASO) airborne instrument: Retrieval algorithm and measurements during DISCOVER-AQ Texas 2013, Atmos. Meas. Tech., 9, 2647–2668, https://doi.org/10.5194/amt-9-2647-2016, 2016.

Nowlan, C. R., (2018), Nitrogen dioxide and formaldehyde measurements from the GEOstationary Coastal and Air Pollution Events (GEO-CAPE) Airborne Simulator over Houston, Texas, Atmos. Meas. Tech., 11, 5941–5964, https://doi.org/10.5194/amt-11-5941-2018, 2018.

https://doi.org/10.5194/egusphere-2023-152
Preprint. Discussion started: 2 February 2023

Morrison, H., J. A. Curry, V. I. Khvorostyanov (2005), A new double-moment microphysics parameterization for application in cloud and climate models. Part 1: Description, *J. Atmos. Sci., 62*, 1665-1677, doi:10.1175/JAS3446.1.

National Emissions Inventory Collaborative (2019). 2016v1 Emissions Modeling Platform. Retrieved from http://views.cira.colostate.edu/wiki/wiki/10202.

Nault, B. A., J. L. Laughner, P. J. Wooldridge, J. D. Crounse, J. Dibb, G. Diskin J. Peischl, J. R. Podolske, I. B. Pollack, T. B. Ryerson, E. Scheuer, P. O. Wennberg, and R. C. Cohen (2017), Lightning NOx emissions: Reconciling Measured and Modeled Estimates with Updated NOx Chemistry, *Geophys. Res. Lett., 44*(18), 9479-9488, doi:10.1002/2017GL074436.

Nolte, C. G., K. W. Appel, J. T. Kelly, P. V. Bhave, K. M. Fahey, J. L. Collett, L. Zhang, and J. O. Young (2015), Evaluation of the Community Multiscale Air Quality (CMAQ) model v5.0 against size-resolved measurements of inorganic particle composition across sites in North America, *Geosci. Model Dev.*, *8*(9), 2877–2892, doi:10.5194/gmd-8-2877-2015.

Pierce, R. B., T. Schaack, J. A. Al-Saadi, T. D. Fairlie, C. Kittaka, G. Lingenfelser, M. Natarajan, J. Olson, A. Soja, T. Zapotocny, A. Lenzen, J. Stobie, D. Johnson, M. A. Avery, G. W. Sachse, A. Thompson, R. Cohen, J. E. Dibb, D. Rault, R. Martin, J. Szykman, and J. Fishman (2007), Chemical data assimilation estimates of continental U.S. ozone and nitrogen budgets during the Intercontinental Chemical Transport Experiment-North America, *J. Geophys. Res. Atmos., 112*(D12), doi:10.1029/2006JD007722.

Pleim, J. E. (2007), A combined local and nonlocal closure model for the atmospheric boundary layer. Part I: Model description and testing, *J. Appl. Meteorol. Climatol., 46*(9), 1383-1395, doi:10.1175/JAM2539.1.

Schwab, D. J., G. A. Leshkevich, and G. C. Muhr (1992), Satellite measurements of surface water temperature in the Great Lakes: Great Lakes Coastwatch, *J. Great Lakes Res., 18*(2), 247-258, doi:10.1016/S0380-1330(92)71292-1.

Sexton, K., and H. Westberg (1980), Elevated Ozone Concentrations Measured Downwind of the Chicago-Gary Urban Complex, *J. Air Pollut. Control Assoc., 30*(8), 911-914, doi:10.1080/00022470.1980.10465132.

Shindell, D., J. C. I. Kuylenstierna, E. Vignati, R. Van Dingenen, M. Amann, Z. Klimont, S. C. Anenberg, N. Muller, G. Janssens-Maenhout, F. Raes, J. Schwartz, G. Faluvegi, L. Pozzoli, K. Kupiainen, L. Höglund-Isaksson, L. Emberson, D. Streets, V. Ramanathan, K. Hicks, N. T. K. Oanh, G. Milly, M. Williams, V. Demkine, and D. Fowler (2012), Simultaneously Mitigating Near-Term Climate Change and Improving Human Health and Food Security, *Science, 335*(6065), 183-189, doi: 10.1126/science.1210026.

Thompson, G., P. R. Field, R. M. Rasmussen, and W. D. Hall (2008), Explicit forecasts of winter precipitation using an improved bulk microphysics scheme. Part II: Implementation of a new snow parameterization, *Mon. Wea. Rev., 136*(12), 5095-5115, doi:10.1175/2008MWR2387.1

Thompson, G., M. Tewari, K. Ikdea, S. Tessendorf, C. Weeks, J. Otkin, and F. Kong (2016), Explicitly-coupled cloud physics and radiation parameterizations and subsequent evaluation in WRF high-resolution convective forecasts, *Atmos. Res., 168*, 92-104, doi:10.1016/j.atmosres.2015.09.005.

US Environmental Protection Agency (2021), 2017 National Emissions Inventory: January 2021 Updated Release, Technical Support Document, EPA-454/R-21-001, retrieved from https://www.epa.gov/sites/default/files/2021-02/documents/nei2017_tsd_full_jan2021.pdf

Vargas, M., Z. Jiang, J. Ju, and I. A. Csiszar (2015), Real-time daily rolling weekly Green Vegetation Fraction (GVF) derived from the Visible Infrared Imaging Radiometer Suite (VIIRS) sensor onboard the SNPP satellite, 20th Conf. Satellite Meteorology and Oceanography, Phoenix AZ, Amer. Meteor. Soc., P210, retrieved from https://ams.confex.com/ams/95Annual/webprogram/Paper259494.html

Wang, K., Y. Zhang, S. Yu, D. C. Wong, J. Pleim, R. Mathur, J. T. Kelly, and M. Bell (2021), A comparative study of two-way and offline coupled WRF v3.4 and CMAQ v5.0.2 over the contiguous US: performance evaluation and impacts of chemistry-meteorology feedbacks on air quality, *Geosci. Model Dev., 14*, 7189-7221, doi: 10.5194/gmd-14-7189-2021

Wagner, Timothy J., et al. "Observations of the Development and Vertical Structure of the Lake-Breeze Circulation during the 2017 Lake Michigan Ozone Study." Journal of the Atmospheric Sciences 79.4 (2022): 1005-1020.

Xiu, A., and J. E. Pleim (2001), Development of a land surface model. Part I: Application in a mesoscale meteorological model, *J. Appl. Meteor., 40*(2), 192-209, doi:10.1175/1520-0450(2001)040<0192:DOALSM>2.0.CO;2.